RESEARCH ARTICLE

Asian Research Association

INTERNATIONAL RESEARCH JOURNAL OF
MULTIDISCIPLINARY TECHNOVATION

DOI: 10.54392/irjmt2419

Exploration of Solvent Effects, Structural and Spectroscopic Properties, Chemical Shifts, Bonding Nature, Reactive Sites and Molecular Docking Studies on 3-Chloro-2,6-Difluoropyridin-4-Amine as a Potent Antimicrobial Agent

S. Kavi Karunya [a,*], K. Jagathy [b], K. Anandaraj [a], C. Pavithra [c], R. Manjula [c,d]

[a] PG and Research Department of Microbiology, Shanmuga Industries Arts and Science College, Tiruvannamalai-606603, Tamil Nadu, India.
[b] PG and Research Department of Microbiology, Sri Akilandeswari Women's College, Wandiwash, Tiruvannamalai-604408, Tamil Nadu, India.
[c] PG and Research Department of Physics, Marudhar Kesari Jain College for Women, Vaniyambadi-635751, Tamil Nadu, India.
[d] Department of Physics, Sri Aandal Arts and Science College for Women, Kilmurungai, Ambur-635 812, Tamil Nadu, India.
* Corresponding Author Email: kavi.vit@gmail.com

DOI: https://doi.org/10.54392/irjmt2419
Received: 04-11-2023; Revised: 12-01-2024; Accepted: 20-01-2024; Published: 30-01-2024

Abstract: This study delved into the electronic structure of Pyridine derivative 3-Chloro-2,6-difluoropyridin-4-amine (3C26D4A) using quantum-chemical computational calculations and employing the DFT/B3LYP/6-311++G(d,p) method and basis set. Spectroscopic, electronic, Mulliken population analysis and molecular electrostatic potential surface (MESP) calculations were carried out to gain deeper insights, shedding light on their bonding characteristics and reactive sites. The simulated electronic and frontier molecular orbitals (FMO) energy gaps of 3C26D4A in both polar (aniline, DMSO and methanol) and nonpolar (CCl_4, chloroform, cyclohexane and toluene) confirm the stability and chemical reactivity. The highest occupied molecular orbital (HOMO) and lowest unoccupied molecular orbital (LUMO) energy gap of 3C26D4A in the gas phase is found to be 6.0214 eV and shows low reactivity and stability as compared to the solvent phase. In parallel, in silico molecular docking investigated their promise as antimicrobial agents by targeting key enzyme DNA gyrase. The obtained binding energy revealed a significant inhibitory potential docking score of -4.07 kcal/mol.

Keywords: Pyridine Derivative, DFT, Solvent effect, Molecular docking, DNA Gyrase

1. Introduction

Pyridine, with the molecular formula C_5H_5N, is a fundamental heterocyclic compound crucially present in various natural compounds. The structure of pyridine shares multiple similarities with benzene, as a nitrogen atom takes the place of a C-H group within the benzene structure [1-3]. Pyridine derivatives have potential antimicrobial, anti-diabetic, anti-oxidant and anti-proliferative activities [4-7]. Due to the increased affinity with metal ions, pyridine derivatives have been utilized to detect environmental pollution [8, 9]. At the same time, fluorinated components play a pivotal role in drug discovery due to increased electronegativity by attracting electrons, making them essential elements in the structural composition of a wide array of drugs [10]. 3-Chloro-2,6-difluoropyridin-4-amine (3C26D4A) alternatively goes by the name of 4-amino-3-chloro-2,6-difluoropyridin with a molecular formula of $C_5H_3ClF_2N_2$ and molecular mass of 164.54 g/mol with one and four hydrogen bond donor and acceptors respectively. From the structure of the fluorinated compound, 3C26D4A comprises an aromatic ring, fluorine (F), chlorine (Cl), and amino groups (NH_2) anchored to the pyridine structure. The amino group stems from the pyridine structure at *ortho* and *meta* positions concerning chlorine and fluorine atoms. At the same time, chlorine and fluorine atoms are connected to the pyridine structure at *ortho* and *meta* positions involving amino groups. The spectroscopic properties of dimethyl pyridines have been reported earlier [11]. Furthermore, the molecular structure of 3-methyl pyridine in gas, liquid, and solid states has been studied using Raman spectroscopy [12]. The calculated and experimental spectroscopic studies on mono, di and trimethyl pyridines were reported using a theoretical RHF/3-21G basis set and compared with experimental values [13].

DNA gyrase, also identified as type IIA topoisomerase found within bacterial cells, is renowned for its ability to generate negative supercoils through the cleavage of both strands in a DNA segment (G-DNA),

resulting in the separation of the strands. As a moonlighting protein with diverse regulatory functions in bacteria, DNA gyrase plays a crucial role in influencing processes like replication and transcription by modulating the availability of DNA molecules, thereby affecting their binding with DNA and RNA polymerase enzymes. The absence of DNA-gyrase in higher eukaryotes renders it a promising target for antibiotics [14-16]. Pyridine and its derivatives showcase extensive applications in medicinal chemistry, making it imperative to comprehend the chemical reactivity and various structural aspects. After reviewing existing literature, it was found that 3C26D4A has not undergone any theoretical spectroscopic studies. Considering this gap, the current research aims to extensively characterize the titled compound using a quantum computational approach, Density function Theory (DFT), to provide a better understanding of the electronic, structural, pharmacokinetic and biological attributes of 3C26D4A.

2. Computational Details

The quantum-chemical simulations of 3C26D4A were executed using Gaussian 09W software. The analysis employed density functional theory (DFT) at the B3LYP level, utilizing the 6-311++G(d,p) basis set. Notably, the computations were conducted without imposing any restrictions on the molecular geometry [17-20] and the findings were integrated with the results obtained from the Chemcraft program [21]. Additionally, the chemical shifts and electronic properties of 3C26D4A were simulated utilizing Gauge-Invariant Atomic Orbital (GIAO) and Time-Dependent Density Functional Theory (TD-DFT) with the same basis set [22-25]. The crystal structure of macromolecule (protein) DNA gyrase with a PDB ID of 1KZN featuring a resolution of 2.30 Å was obtained from the Protein Data Bank (PDB). The bound ligand and water molecules in the crystal structure of the macromolecule have been removed by utilizing the PyMOL graphics tool and saved in PDB format [26]. The GaussView 6.0 program was employed to build the crystal structure of 3C26D4A and formatted it into a PDB file [27]. The interaction of macromolecule and ligand, polar and nonpolar bonding and binding energy were simulated using AutoDock software and calculated using the LigPlot+ program [28, 29].

3. Results and Discussion

3.1. Optimized Molecular Geometry

The simulated molecular structure of 3C26D4A and the numbering of atoms are illustrated in Figure. 1 and the features of the simulated geometric parameters are presented in Table 1. However, as the crystal structure of 3C26D4A remains inaccessible, the analysis involves comparisons with compounds structurally akin to them [30]. In 3C26D4A has one Cl-C and C-H, two F-C and N-H, three N-C, and four C-C bond distances, as well as two C-C-C, C-N-H, F-C-C, F-C-N and Cl-C-C, one C-N-C and H-N-H, three C-C-H and four N-C-C bond angles. From the findings, the simulated bond distances of carbon atoms fall between 1.379-1.412 Å, aligning closely with the observed range of 1.372-1.409 Å. The bond interval of C-H and Cl-C were calculated at 1.082 and 1.746 Å, and the corresponding experimental value was measured at 1.721 Å for Cl-C. Moving the bond interval of N-H in the amino group and F-C were calculated between 1.006-1.007 Å and 1.336-1.345 Å and the conforming experimental findings fall between 0.838-0.848 Å and 1.335-1.336 Å respectively. Similarly, the bond interspace of N-C was simulated between 1.314-1.362 Å and observed at 1.312-1.342 Å. The bond angles of C-N-C and H-N-H were simulated at 119.5 and 124.4 ◦ and observed at 124.4 and 114.1◦, respectively. In contrast, with other bond lengths, the bond distance of Cl_1-C_7 is increased, resulting in a weaker bond distance attributed to an electronegative group in the adjacent position.

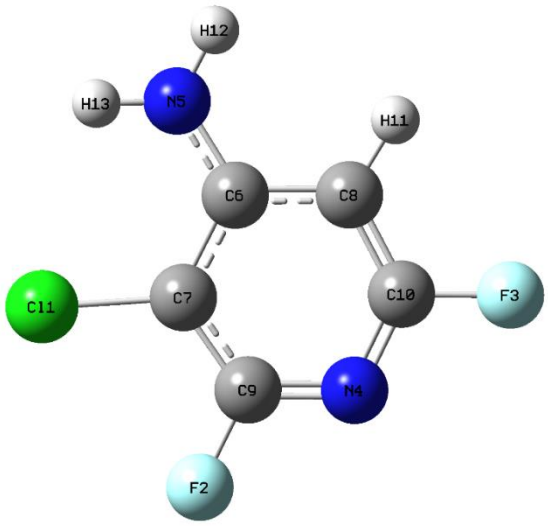

Figure 1. Optimized molecular structure of 3C26D4A in the gas phase

Table 1. Calculated and observed geometrical parameters of 3C26D4A

Bond lengths (Å)	DFT	Exp*	Bond lengths (Å)	DFT	Exp*
Cl_1-C_7	1.746	1.721	N_5-H_{13}	1.007	0.838
F_2-C_9	1.336	1.336	C_6-C_7	1.412	1.405
F_3-C_{10}	1.343	1.335	C_6-C_8	1.407	1.409
N_4-C_9	1.314	1.319	C_7-C_9	1.387	1.368
N_4-C_{10}	1.316	1.312	C_8-C_{10}	1.379	1.372
N_5-C_6	1.362	1.342	C_8-H_{11}	1.082	-
N_5-H_{12}	1.006	0.848	-	-	-
Bond angles (◦)	**DFT**	**Exp***	**Bond angles (◦)**	**DFT**	**Exp***
Cl_1-C_7-C_6	120.6	120.7	C_6-N_5-H_{13}	119.4	121.3
Cl_1-C_7-C_9	121.3	120.6	N_5-C_6-C_7	121.4	122.0
F_2-C_9-N_4	116.1	115.2	N_5-C_6-C_8	121.5	122.1
F_2-C_9-C_7	118.7	118.6	H_{12}-N_5-H_{13}	117.3	114.1
F_3-C_{10}-N_4	115.6	114.7	C_7-C_6-C_8	117.1	115.8
F_3-C_{10}-C_8	118.1	119.0	C_6-C_7-C_9	118.1	118.6
C_9-N_4-C_{10}	115.8	114.7	C_6-C_8-H_{10}	117.5	118.4
N_4-C_9-C_7	125.2	126.0	C_6-C_8-H_{11}	121.7	-
N_4-C_{10}-C_8	126.3	126.2	C_{10}-C_8-H_{11}	120.8	-
C_6-N_5-H_{12}	119.5	124.4	-	-	-

***** Taken from Ref [30]

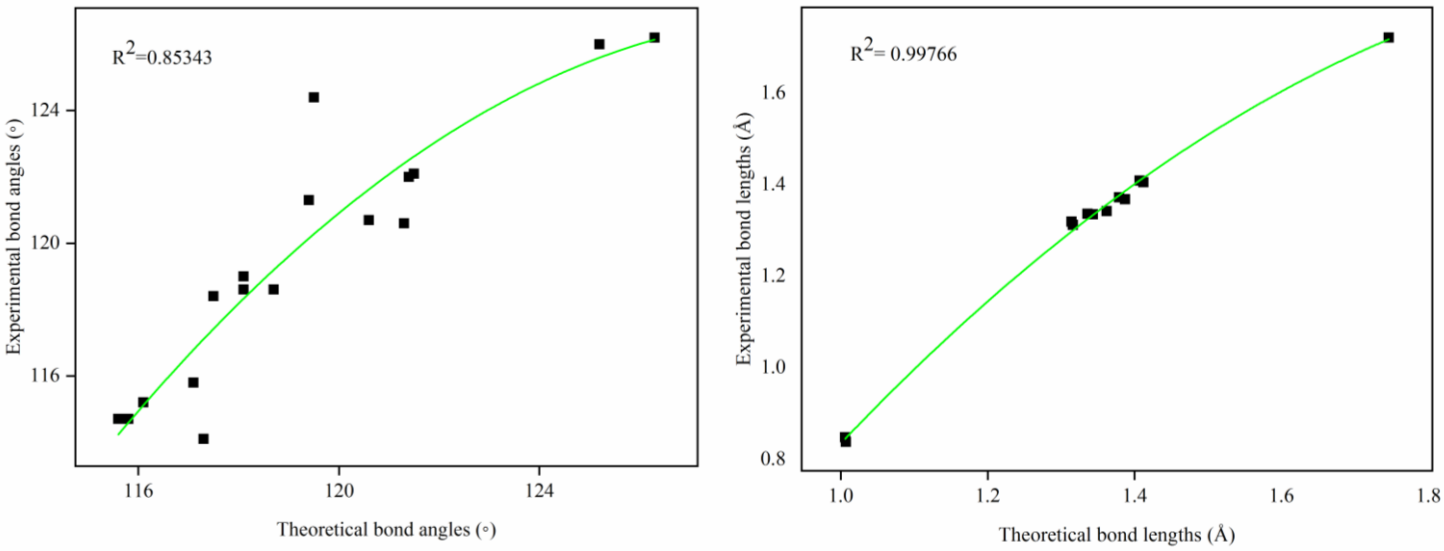

Figure 2. Correlation graph for calculated and experimental bond lengths and bond angles of 3C26D4A

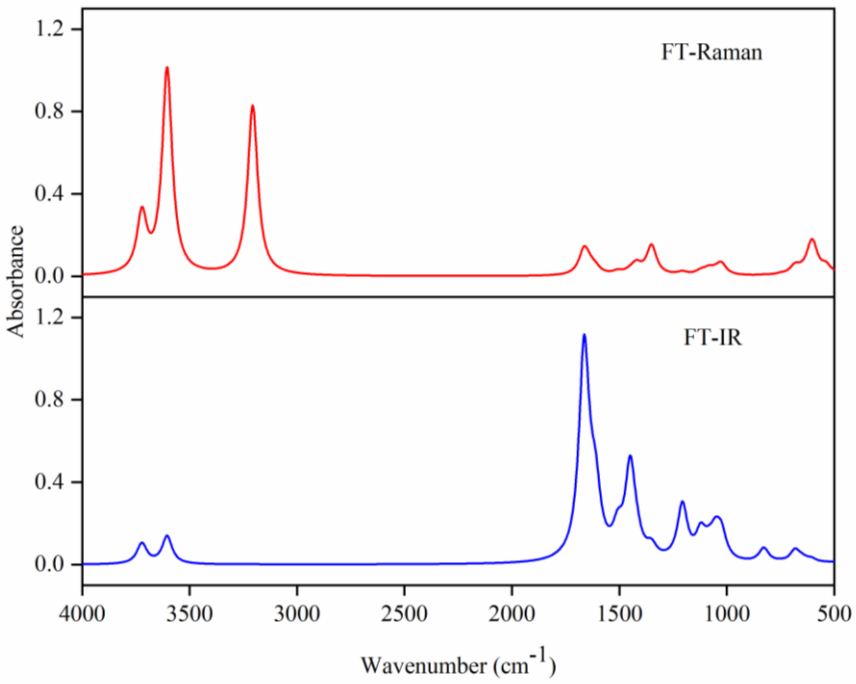

Figure 3. Simulated FT-IR and FT-Raman spectra of 3C26D4A

Whereas in C-C-C, C-N-H, F-C-C, F-C-N and Cl-C-C were simulated between 117.1-118.1, 119.4-119.5, 118.1-118.7, 115.6-116.1 and 120.6-121.3◦ and observed between 115.8-118.6, 121.3-124.4, 118.6-119.0, 114.7-115.2 and 120.6-120.7◦ respectively. Similarly, C-C-H and N-C-C bond angles were simulated within the range of 117.5-120.8 and 121.4-126.3◦ and observed at 118.4 and 122.0-126.2◦, respectively. Figure 2 displayed the correlation graphs among the theoretical and experimental bond distances and angles. These exhibited a good contract with the observed values, showcasing a robust linear coefficient R^2 of 0.99766 (bond distance) and 0.85343 (bond angles). These outcomes indicate the proximity between experimental and theoretical values for 3C26D4A.

3.2. Vibrational Analysis

3C26D4A contains 13 atoms and 33 fundamental modes of vibrations as per the expected (3N-6) degrees of freedom characteristic of C1 symmetry. The calculated vibrational (FT-IR and Raman) spectra of 3C26D4A were visualized in Figure. 3 and the corresponding wavenumbers were presented in Table 2 and modified with a scaling factor of 0.96 [31].

3.2.1. Stretching vibrations

3C26D4A has an amino group (NH_2) stem from the pyridine structure carbon atom at *ortho* and *meta* positions concerning chlorine and fluorine atoms. The symmetric and asymmetric stretching vibrations of an amino group (NH_2) were anticipated to fall in 3450-3250 and 3550-3330 cm^{-1} [32]. In the present study, the amino group stretched asymmetric vibrations at 3573 and 3460 cm^{-1} with a PED value of 100%. Identifying the stretching vibration of C-F is closely linked to the in-plane deformations of the functional group. The C-F stretching of two and four fluoroanilines was simulated at 1194 and 1223 cm^{-1} in the literature [33]. In 3C26D4A, C-F stretching was simulated at 1363 and 1158 cm^{-1} with a PED value of 34 and 22%, respectively. The C-H stretchings are predicted within the 3100-3000 cm^{-1} [34, 35]. According to this report, the C-H stretching of 3C26D4A was simulated at 3078 cm^{-1} with a PED value of 99%. The chlorine atom connected to the pyridine structure at the *ortho* position of amino (NH_2) and fluorine (F) atoms gives rise to stretching vibrations at 1041 and 654 cm^{-1}.

3.2.2. Bending vibrations

3C26D4A has a C-H group in the pyridine structure at *ortho* and *meta* positions concerning amino, fluorine, and chlorine atoms, which were anticipated to fall within the range of 1450-1000 cm^{-1} and 1000-750 cm^{-1} for in-plane and out-of-plane deformations respectively [36, 37]. The present work simulated the C-H in-plane and out-of-plane deformations at 1158, 1011 cm^{-1}, and 984 cm^{-1} with a PED contribution of 49, 12, and 44%, respectively. The amino group stems to the ring structure at the *ortho* and *meta* positions of hetero atoms, giving rise to deformations at 1597 and 1572 cm^{-1} with a PED value of 17 and 44%, respectively. The C-F in-plane deformations of fluoro aniline isomers were simulated at 562 and 591 cm^{-1} [38]. In line with this observation, the C-F deformations were simulated at 588 and 516 cm^{-1} with a PED value of 14 and 10%, respectively. The

simulated values show significant coincidences with the literature.

Table 2. Simulated vibrational wave numbers and assignments of 3C26D4A

Modes	Theoretical wave numbers (cm^{-1})		I_{IR}	I_{Raman}	Vibrational assignments (≥ 10% PED)
	Unscaled	Scaled			
1	3722	3573	55.11	37.47	υ_{as} NH_2 (100)
2	3604	3460	74.23	132.8	υ_{as} NH_2 (100)
3	3206	3078	0.45	109.5	υ CH (99)
4	1664	1597	551.2	16.09	υ CC (14), χ NH_2 (17)
5	1638	1572	44.03	4.09	υ CC (26), χ NH_2 (44)
6	1610	1546	152.9	3.42	υ CN (30), υ CC (24), β CCN (11)
7	1507	1447	67.72	2.04	υ CN (25), β HCC (17)
8	1449	1391	243.3	1.76	υ CC (47)
9	1420	1363	34.00	6.37	υ CN (31), υ FC (34)
10	1350	1296	30.74	19.03	υ CN (24), υ CC (48), β HNC (11)
11	1206	1158	148.9	1.90	υ CN (26), υ FC (22), β HCC (49)
12	1121	1076	68.65	2.39	υ FC (12), β HNC (38)
13	1084	1041	27.36	3.57	υ FC (28), υ ClC (16), β CCN (21)
14	1053	1011	61.81	1.59	υ CN (12), υ CC (14), β HNC (14), β HCC (12)
15	1025	984	67.93	7.31	υ CC (13), β HNC (16), β HCC (44)
16	827	794	37.87	0.21	τ HCCN (60), τ FCNC (15), τ NCCC (15)
17	750	720	1.84	0.60	τ HCCN (14), τ CNCC (10), τ CCNC (32), τ FCNC (22)
18	684	657	0.32	1.24	τ FCNC (50), τ NCCC (15)
19	681	654	32.72	4.04	υ ClC (22), β CCN (17), β FCN (33)
20	648	622	9.03	0.68	τ HCCN (11), τ FCNC (43), τ NCCC (32)
21	612	588	5.67	7.58	β FC (14), β CCC (18)
22	599	575	3.81	15.58	β CCN (10), β NCC (15)
23	538	516	0.70	5.12	β CNC (26), β CCC (23), β FC (10)
24	449	431	6.50	0.39	τ HNCC (89)
25	407	391	2.02	6.40	β CCN (30), β FCN (12)
26	344	330	1.08	0.84	β NCC (11), β ClCC (68)
27	328	315	2.31	0.24	β NCC (11), β FCN (63)
28	315	302	2.81	1.14	β NCC (40), β FCN (14)
29	255	245	198.2	3.10	τ HNCC (79)
30	240	230	33.13	1.16	τ CNCC (13), τ CCNC (26), τ CCCN (18), τ FCNC (18)
31	228	219	3.63	1.35	β CCN (11), β ClCC (72)
32	204	196	1.78	0.50	τ CNCC (12), τ CCCN (36), τ FCNC (29)
33	98	94	0.31	0.15	τ CNCC (44), τ CCNC (21), τ CCCN (22), τ ClCCC (11)

υ - stretching, υ_{as} - asymmetric stretching, β- deformation. The theoretical wavenumber scaling factor for all vibrations is 0.96

3.3. Chemical shifts

Combining NMR spectroscopy with quantum computational chemical techniques offers a promising avenue for advancing the understanding of organic molecule structures. The theoretical ^{1}H and ^{13}C chemical shifts for 3C26D4A, outlined in Table 3, viewed in Figs. 4 and 5 and aligned with Figure. 1 atom numbering, serve as a valuable reference. Typically, in the ^{1}H NMR spectrum, the chemical shifts of aromatic protons ^{1}H and ^{13}C carbon fall within the range of 7.00-8.00 ppm and 100-150 ppm, respectively [39, 40]. In the case of 3C26D4A, protons (H_{12} and H_{13}) in the amino group (NH_2) were simulated at 3.92 and 4.36 ppm. Similarly, the proton (H_{11}) attached to the ring structure was simulated at 5.77 ppm. The simulated chemical shifts were lower than the standard range, primarily due to the deshielding effects caused by the presence of electronegative chlorine and fluorine atoms in the ortho positions of the protons. The simulated chemical shift of the carbon atoms in the ring structure was between 92.52 and 168.22 ppm. Notably, the simulated chemical shift of carbons C_6 (158.52), C_9 (165.20) and C_{10} (168.22) were found to be elevated compared to the standard range. This increase is attributed to the

influence of nitrogen and fluorine atoms stemming from these specific carbon positions. Consequently, an endeavor was made to align DFT values with the predictions generated by ChemDraw. Remarkably, most of the theoretical values closely matched the predictions made by ChemDraw Ultra 12.0.

Table 3. Theoretical 1H and 13C NMR chemical shifts (ppm) of 3C26D4A

DFT		ChemDraw	
C_6	158.52	C_6	167.3
C_7	107.34	C_7	103.4
C_8	92.52	C_8	95.9
C_9	165.20	C_9	155.4
C_{10}	168.22	C_{10}	162.1
H_{11}	5.77	H_{11}	6.85
H_{12}	3.92	H_{12}	6.27
H_{13}	4.36	H_{13}	6.27

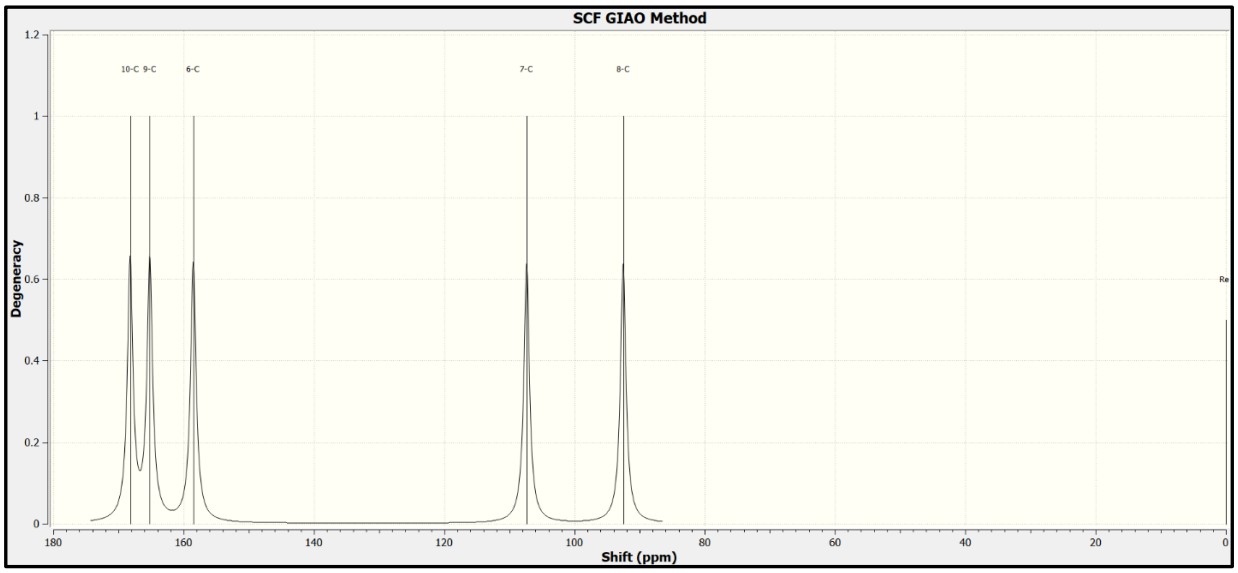

Figure 4. Simulated chemical shift of carbon atoms in the gas phase

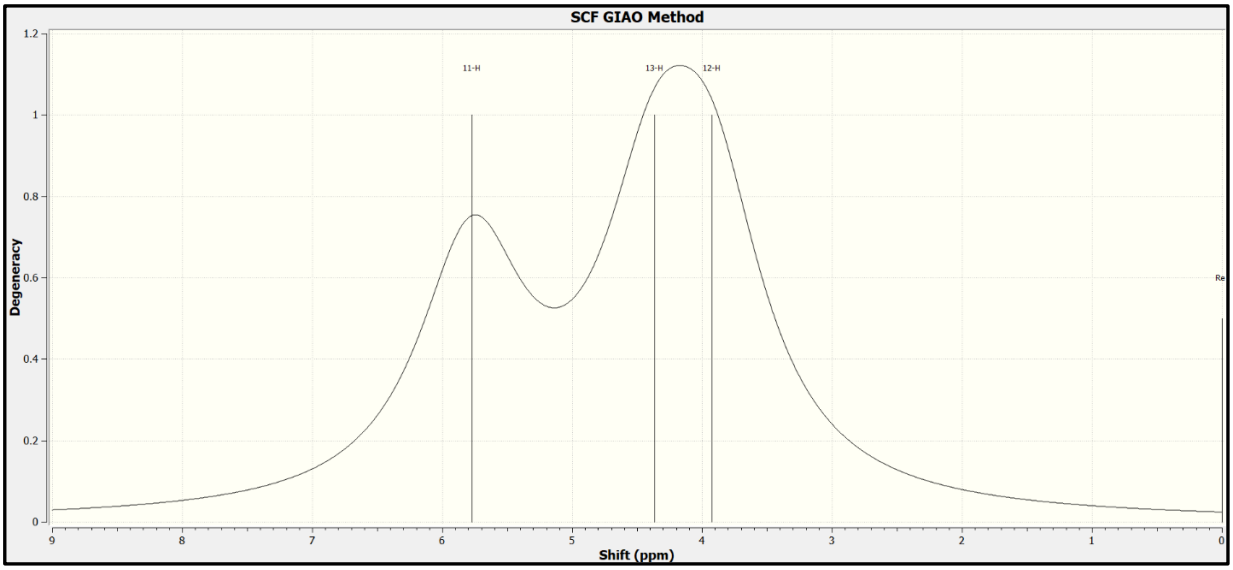

Figure 5. Simulated Chemical Shift of Hydrogen Atoms in the Gas Phase

3.4. Influence of solvents on electronic properties

The electronic (oscillator strength, wavelength and excitation energy) and molecular properties (chemical softness, hardness, electronegativity and affinity) of 3C26D4A were simulated in the gas and solvents (polar and nonpolar) phases are presented in Tables 4, 5 and 6. The simulated electronic spectra of 3C26D4A show six distinct absorptions at 241, 228, 218, 215, 208 and 204 nm as strong to weak bands in the gas phase. The strong peak at 204 nm is attributed to HOMO-1 to LUMO transition of 52%, and the moderate peak at 218 nm is attributed to HOMO to LUMO+1 transition of 47%. In polar solvents (aniline, DMSO and methanol), the bands simulated at 202 nm (aniline) and 201 nm (DMSO and methanol) attributed to HOMO-1 to LUMO+2 transition. As well the nonpolar solvents (CCl_4, chloroform, cyclohexane and toluene) were simulated at 203 nm (CCl_4, cyclohexane and toluene) and 202 nm (chloroform) attributed to HOMO-1 to LUMO+2 transition. The calculated electronic spectra and the corresponding values are presented in Table 5 and visualized in Figure 6.

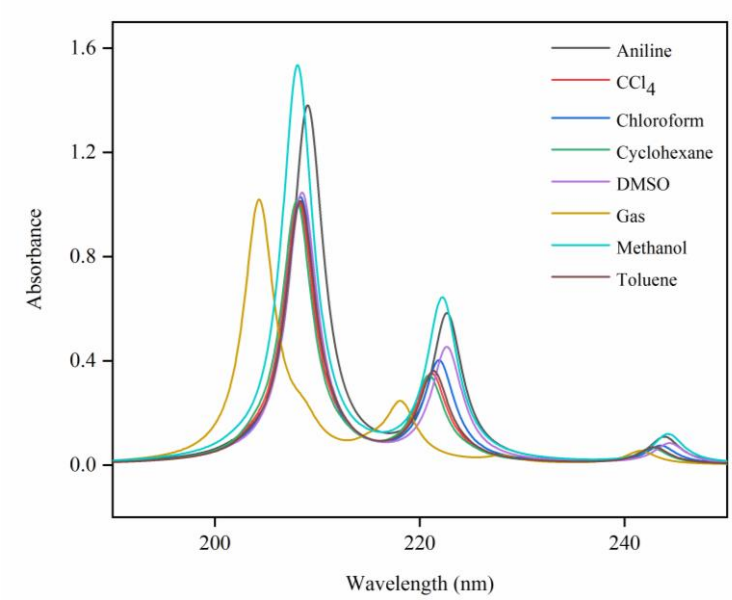

Figure 6. Simulated electronic spectra of 3C26D4A

Table 4. Frontier molecular orbitals and global parameters of 3C26D4A

Parameters	Formula	Gas	CCl_4	DMSO	Cyclohexane	Methanol	Chloroform	Toulene	Aniline
E_{LUMO} (eV)	-	-1.09716	-1.03512	-0.98832	-1.04029	-0.98941	-1.00927	-1.03213	-1.00192
E_{HOMO} (eV)	-	-7.1185	-7.03224	-6.93428	-7.04095	-6.937	-6.398353	-7.02707	-6.96748
$E_{HOMO-LUMO}$ gap(eV)	-	6.02134	5.99712	5.94596	6.00066	5.9476	5.97426	5.99494	5.96556
Ionization potential (I)	$-E_{HOMO}$	7.1185	7.03224	6.93428	7.04095	6.937	6.398353	7.02707	6.96748
Electronegativity (χ)	(I+A)/2	4.1078	4.03368	3.9613	4.04062	3.9632	3.9964	4.0296	3.9847
Electron affinity (A)	$-E_{LUMO}$	1.09716	1.03512	0.98832	1.04029	0.98941	1.00927	1.03213	1.00192
Chemical softness (s)	1/2η	0.08304	0.08337	0.08409	0.08332	0.08407	0.08369	0.0834	0.08381
Chemical potential (μ)	-χ	-4.1078	-4.03368	-3.9613	-4.04062	-3.9632	-3.9964	-4.0296	-3.9847
Global Electrophilicity (ω)	$\mu^2/2\eta$	1.40121	1.35653	1.31954	1.3604	1.32045	1.33667	1.35428	1.33079
Chemical hardness (η)	I-A	6.02134	5.99712	5.94596	6.00066	5.9476	5.97426	5.99494	5.96556

Maximum electron charge (ΔNmax)	−(μ/η)	0.682213	0.672603	0.666217	0.673363	0.666354	0.668936	0.672166	0.667951

Table 5. Calculated electronic properties of 3C26D4A in polar solvents

	λ (nm)	E (eV)	F	Major contributions	Minor contributions
Gas	241	5.1323	0.0111	H→L (56%), H-1→L+1 (24%), H→L+1 (14%)	H-1→L (5%)
	228	5.4369	0.0051	H→L+2 (88%)	H→L+3 (5%)
	218	5.6834	0.0477	H→L (14%), H-1→L (25%), H→L+1 (47%)	H-1→L+1 (2%), H→L+3 (6%)
	215	5.7644	0.0077	H-1→L+2 (21%), H→L+3 (61%)	H→L+1 (6%), H→L+2 (4%), H-1→L+5 (2%)
	208	5.9426	0.0219	H-1→L (10%), H-1→L+2 (59%), H→L+3 (14%)	H→L+1 (4%), H→L+2 (4%)
	204	6.0686	0.2203	H-1→L (52%), H-1→L+2 (14%), H→L+1 (25%),	-
Aniline	243	5.0835	0.023	H→L (59%), H-1→L+1 (18%), H→L+1 (18%)	H-1→L (4%)
	223	5.5513	0.0022	H→L+2 (89%)	H→L+3 (6%)
	222	5.5685	0.1248	H→L (20%), H-1→L (17%), H→L+1 (59%)	H-1→L+1 (3%)
	209	5.9223	0.0872	H-1→L (16%), H-1→L+2 (11%), H→L+3 (52%)	H→L+1 (5%), H→L+2 (6%), H-1→L+1 (4%)
	208	5.9344	0.2262	H-1→L (45%), H→L+1 (14%), H→L+3 (20%)	H-1→L+1 (9%), H-1→L+2 (3%), H→L+2 (3%)
	202	6.1331	0.0028	H-1→L+2 (76%),	H→L+3 (16%), H-1→L+3 (5%)
DMSO	244	5.0732	0.0217	H→L (59%), H-1→L+1 (17%), H→L+1 (19%)	H-1→L (4%)
	223	5.5553	0.0083	H→L+2 (86%)	H→L+3 (4%)
	222	5.5695	0.1123	H→L (19%), H-1→L (16%), H→L+1 (56%)	H-1→L+1 (3%), H→L+2 (4%)
	208	5.9458	0.2746	H-1→L (58%), H-1→L+2 (15%), H→L+1 (17%)	H→L (3%), H→L+3 (2%)
	207	5.9626	0.0117	H-1→L+2 (13%), H→L+3 (72%)	H→L+5 (3%), H→L+2 (8%)
	201	6.1442	0.0017	H-1→L+2 (77%), H→L+3 (16%)	H-1→L+3 (4%)
Methanol	244	5.0759	0.0201	H→L (59%), H-1→L+1 (17%), H→L+1 (19%)	H-1→L (4%)
	223	5.557	0.0034	H→L+2 (89%)	H→L+3 (5%)
	222	5.58	0.1085	H→L (19%), H-1→L (17%), H→L+1 (58%)	H-1→L+1 (3%)
	208	5.9568	0.1798	H-1→L (39%), H-1→L+1 (10%), H→L+3 (25%)	H→L (2%), H→L+2 (2%), H-1→L+2 (5%)
	207	5.9634	0.0952	H-1→L (20%), H→L+3 (48%)	H-1→L+1 (5%), H-1→L+2 (8%), H→L+2 (6%)
	201	6.1441	0.0016	H-1→L+2 (77%), H→L+3 (16%)	H-1→L+3 (4%)

Table 6. Calculated electronic properties of 3C26D4A in nonpolar solvents

CCl_4	λ (nm)	E (eV)	F	Major contributions	Minor contributions

	242	5.1063	0.0191	H-1→L+1 (21%), H→L (58%), H-→L+1 (16%)	H-1→L (5%)
	224	5.5238	0.0036	H→L+2 (87%)	H→L+3 (8%)
	221	5.6061	0.1001	H-1→L (19%), H→L (19%), H→L+1 (57%)	H-1→L+1 (2%)
	212	5.8449	0.0065	H-1→L+2 (16%), H→L+3 (69%)	H→L+2 (8%), H→L+5 (3%)
	208	5.9558	0.3034	H-1→L (63%), H→L+1 (23%)	H-1→L+1 (6%)
	203	6.0879	0.0076	H-1→L+2 (76%), H→L+3 (16%)	H→L+3 (16%), H-1→L+3 (4%)
Chloroform	243	5.0913	0.0203	H-1→L+1 (19%), H→L (58%), H-→L+1 (18%)	H-1→L (4%)
	223	5.5493	0.0019	H→L+2 (89%)	H→L+3 (7%)
	221	5.5878	0.1107	H-1→L (18%), H→L (19%), H→L+1 (58%)	H-1→L+1 (3%)
	209	5.9071	0.0106	H-1→L+2 (14%), H→L+3 (70%)	H→L+2 (9%), H→L+5 (3%)
	208	5.9513	0.2908	H-1→L (60%), H-1→L+1 (10%)	H→L (2%)
	202	6.1261	0.0029	H-1→L+2 (76%), H→L+3 (16%)	H-1→L+3 (5%)
Cyclohexane	242	5.1091	0.0184	H-1→L+1 (21%), H→L (58%), H-→L+1 (16%)	H-1→L (5%)
	224	5.5176	0.0038	H→L+2 (87%)	H→L+3 (8%)
	220	5.6124	0.0958	H-1→L (20%), H→L (18%), H→L+1 (56%)	H-1→L+1 (2%)
	212	5.8348	0.006	H-1→L+2 (16%), H→L+3 (68%)	H→L+2 (8%), H→L+5 (3%)
	207	5.961	0.2985	H-1→L (63%), H-1→L+1 (23%)	H-1→L+1 (6%)
	203	6.0789	0.0101	H-1→L+2 (76%), H→L+3 (15%)	H-1→L+3 (4%)
Toluene	242	5.1044	0.0197	H-1→L+1 (20%), H→L (58%), H-→L+1 (17%)	H-1→L (5%)
	224	5.527	0.0034	H→L+2 (87%)	H→L+3 (8%)
	221	5.601	0.1039	H-1→L (19%), H→L (19%), H→L+1 (57%)	H-1→L+1 (2%)
	211	5.8509	0.007	H-1→L+2 (16%), H→L+3 (69%)	H→L+2 (8%), H→L+5 (3%)
	208	5.9506	0.3075	H-1→L (63%), H→L+1 (23%)	H-1→L+1 (7%)
	203	6.0929	0.0066	H-1→L+2 (76%), H→L+3 (16%)	H-1→L+3 (5%)

	CCl_4	Chloroform	Cyclohexane	Toluene
HOMO	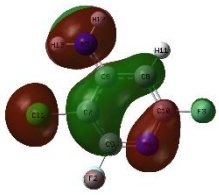	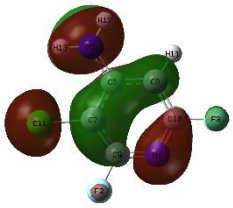	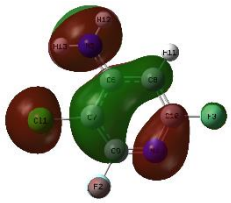	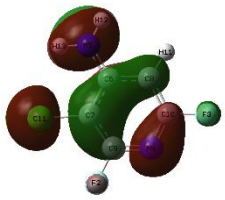
HOMO – LUMO (Eg)	Eg = 5.99712 eV	Eg = 5.97426 eV	Eg = 6.0066 eV	Eg = 5.99494 eV
LUMO	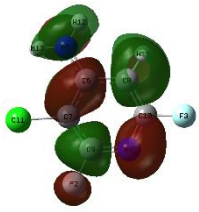	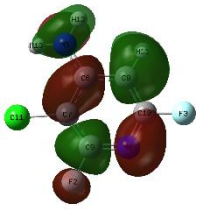	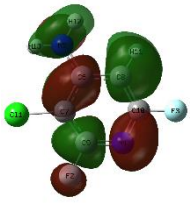	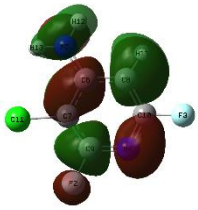

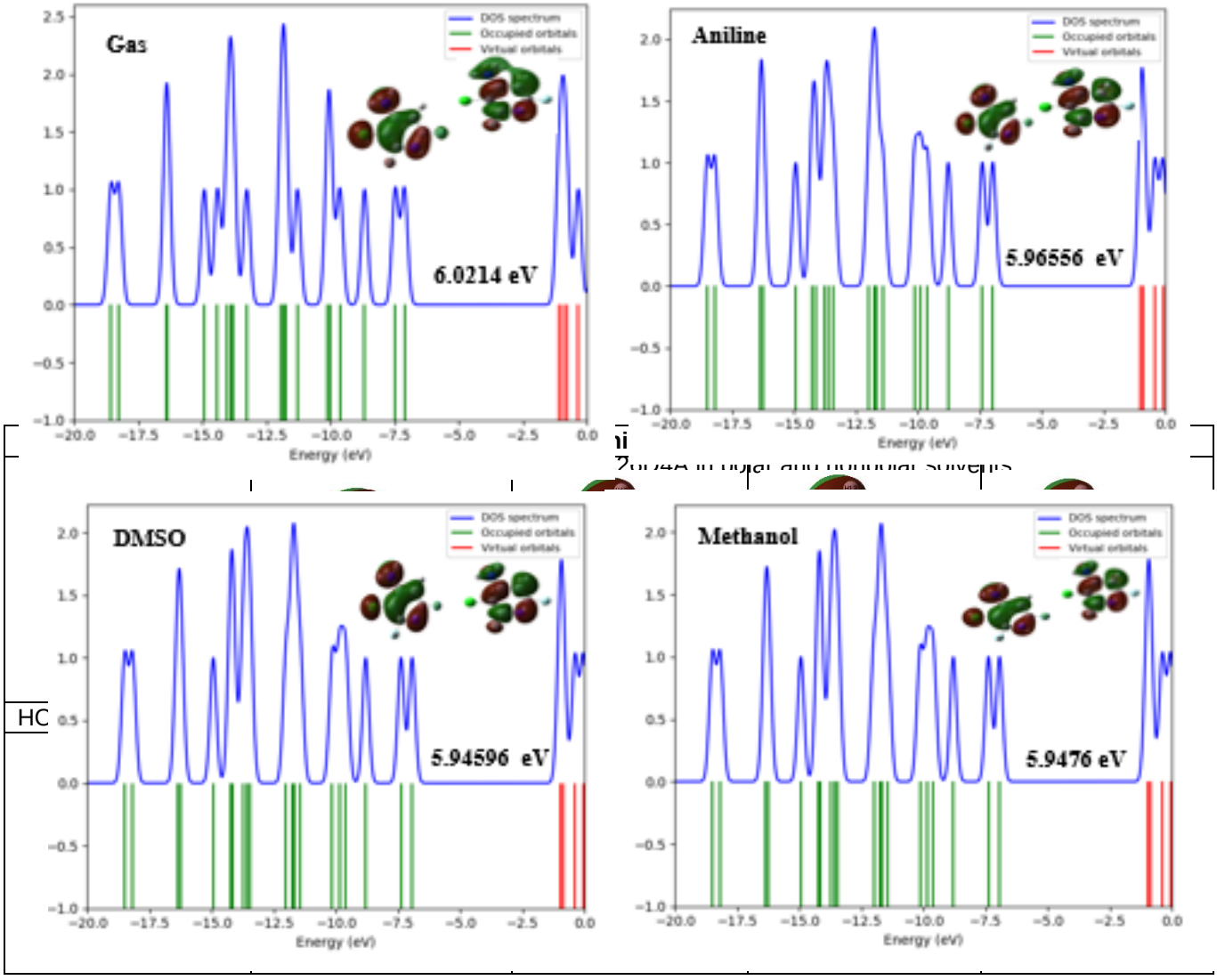

Figure 8. The DOS plots of 3C26D4A in gas and polar solvents

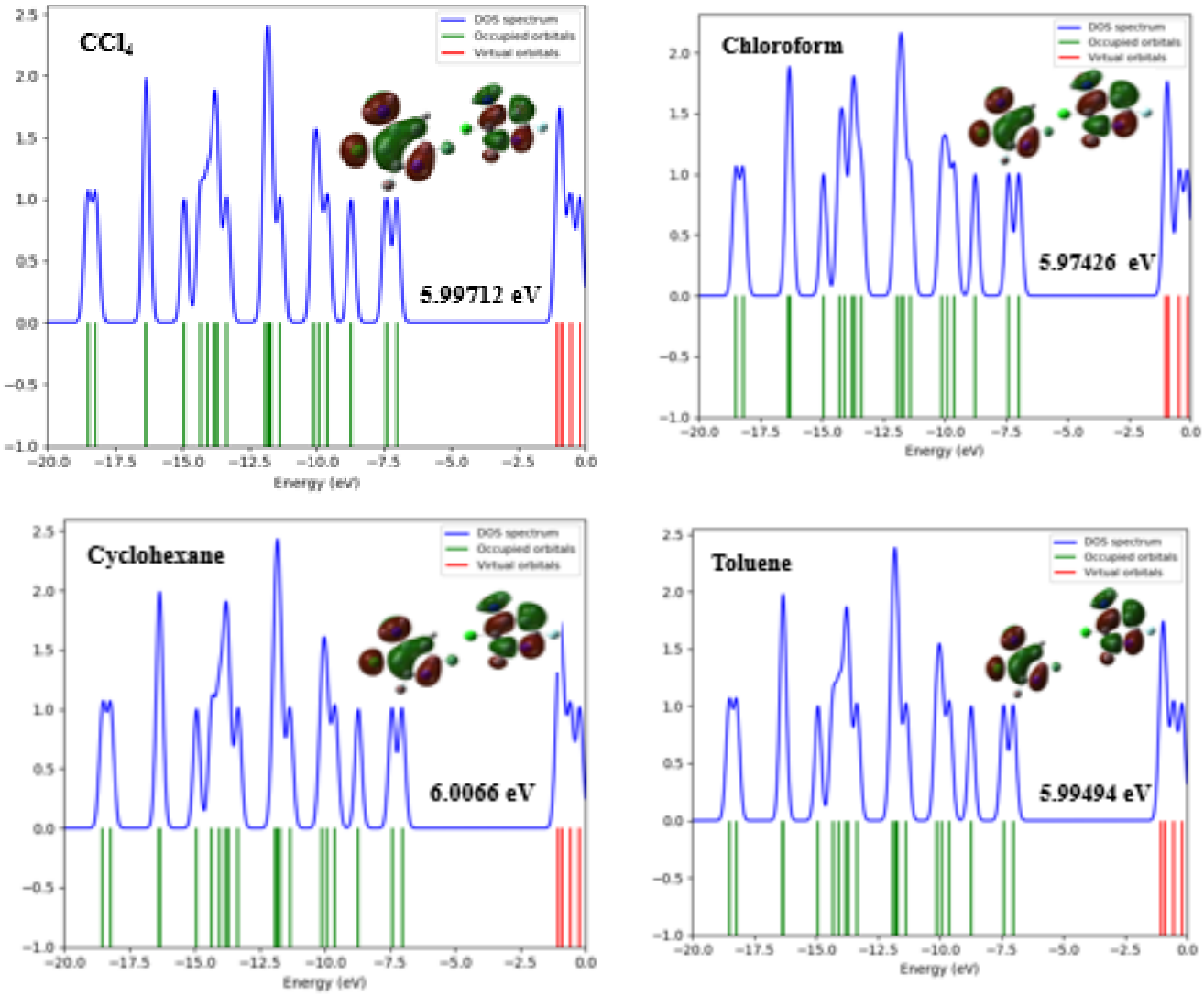

Figure 9. The DOS plots of 3C26D4A in nonpolar solvents

The simulated energy gap in the gas phase of 3C26D4A was 6.0214 eV. The simulated energy gap of polar solvents was 5.96556 eV (aniline), 5.94596 eV (DMSO) and 5.9476 eV (methanol). Similarly, the simulated energy gap for nonpolar solvents was found to be at 5.99712 eV (CCl_4), 5.7426 eV (chloroform), 6.00066 eV (cyclohexane) and 5.99494 eV (toluene). The HOMO-LUMO energy gap and molecular properties are presented in Table 4, pictorially in Figure 7 and the corresponding DOS spectrum was viewed in Figs. 8 and 9. The energy suggests internal charge transfer within the molecule. In nonpolar solvents, chloroform exhibits higher reactivity, while cyclohexane demonstrates lower stability than other nonpolar solvents. Similarly, DMSO and methanol have increased stability and reactivity in polar solvents than aniline. Compared with the gas phase, the slight variations observed in polar and nonpolar solvents show that chemical reactivity and stability have more potential in the solvent phase.

3.5. Natural Bond Orbitals

The molecular structure 3C26D4A underwent an NBO analysis using the DFT/B3LYP method and the 6-311++G (d, p) basis set, as detailed in Table 7. This analytical approach is a practical framework for comprehending intra and intermolecular bonding and transferring charges within the molecular system [41]. In the context of 3C26D4A, the most significant stabilization of interaction energy arises from electron donation occurring from electronegative atom N_5 to the anti-bonding Carbons six and seven characterized by the LP(1)→π* transition, yielding a stabilization energy of 46.61 kJ/mol. Likewise, the second significant contribution from electron endowment from C_6-C_7 to the anti-bonding N_4-C_9 involves the transition of π→π*amounts to 35.79 kJ/mol. On the other hand, the π→π* were also found between the electron donation occurring from N_4-C_9, C_6-C_7, C_8-C_{10}, and C_8-C_{10} to the

anti-bonding C_8-C_{10}, C_8-C_{10}, N_4-C_9 and C_6-C_7 yielding an intramolecular stabilization energy of 31.81, 10.86, 11.84 and 27.13 kJ/mol respectively.

3.6. Mulliken Charge Distributions

The Mulliken charges of 3C26D4A were simulated using the B3LYP/6-311++G(d,p) basis set, yielding specific charges accessible in Table 8 and viewed in Fig 10. The calculation of atomic charges of molecules holds substantial importance in quantum chemical methods. In 3C26D4A, the electronegative atoms revealed net negative charges encompassing F_2 (-0.12908e), F_3 (-0.14717e), N_4 (-0.16487e) and N_5 (-0.19184e). In addition, carbon atoms attached to the amino group and fluorine atoms such as C_6 (-1.50699e), C_9 (-0.11115e) and C_{10} (-0.26568e) have net negative charges by the influence of electronegative atoms. Conversely, the other carbon atoms and hydrogen atoms have net positive charges. Notably, the carbon atom C_7 (1.253034e) attached to chlorine (Cl) has more positive potential than other atoms. The carbon atom C_6 (-1.50699e) linked to the amino group (NH_2) has a more negative potential. Further examination of hydrogen and oxygen atoms in both substances revealed their dual behavior, displaying a combination of positive and negative charges, as verified by MESP analysis.

3.7. Molecular Electrostatic Potential Surface

Molecular electrostatic potential (MESP) surfaces offer valuable insights into potential sites for electrophilic and nucleophilic attacks and hydrogen bonding [42-45]. The surface map of 3C26D4A is illustrated in Fig. 11. The electrostatic possible range for 3C26D4A spans from -7.007×10^{-2} to 7.007×10^{-2} e.s.u (gas), -8.242×10^{-2} to 8.242×10^{-2} (aniline), -7.658×10^{-2} to 7.658×10^{-2} e.s.u (CCl_4), -8.092×10^{-2} to 8.092×10^{-2} e.s.u (chloroform), -7.575×10^{-2} to 7.575×10^{-2} e.s.u (cyclohexane), -8.560×10^{-2} to 8.560×10^{-2} (DMSO), -8.534×10^{-2} to 8.534×10^{-2} (methanol) and -7.703×10^{-2} to 7.703×10^{-2} (toulene). The findings show that the negative regions span around the nitrogen and fluorine electronegative atoms, revealing sites for electrophilic attacks. Meanwhile, positive regions, typically associated with hydrogen atom sites for nucleophilic attacks, are depicted in blue.

Table 7. Donor and acceptor interactions for 3C26D4A

Donor (i)	Type	Acceptor (j)	Type	Type of transition	E(2)[a] (KJ/mol)	E(j)-E(i)[b] (a.u)	F(i,j)[c] (a.u)
N_4-C_9	π	C_8-C_{10}	π*	π- π*	31.81	0.33	0.094
C_6-C_7	π	N_4-C_9	π*	π- π*	35.79	0.27	0.091
C_6-C_7	π	C_8-C_{10}	π*	π- π*	10.86	0.29	0.050
C_8-C_{10}	π	N_4-C_9	π*	π- π*	11.84	0.27	0.053
C_8-C_{10}	π	C_6-C_7	π*	π- π*	27.13	0.27	0.081
Cl_1	LP(3)	C_6-C_7	π*	LP(3)-π*	10.38	0.31	0.057
F_2	LP(3)	N_4-C_9	π*	LP(3)-π*	23.69	0.40	0.097
F_3	LP(3)	C_8-C_9	π*	LP(3)-π*	21.61	0.42	0.092
N_5	LP(1)	C_6-C_7	π*	LP(1)-π*	46.61	0.27	0.108

Table 8. Mulliken population analysis of 3C26D4A in the gas phase

S. No.	Atoms	Charges (e)
1	Cl_1	0.251277
2	F_2	-0.12908
3	F_3	-0.14717
4	N_4	-0.16487
5	N_5	-0.19184
6	C_6	-1.50699
7	C_7	1.253034
8	C_8	0.309213
9	C_9	-0.11115
10	C_{10}	-0.26568
11	H_{11}	0.195377
12	H_{12}	0.260626

13	H_{13}	0.247248

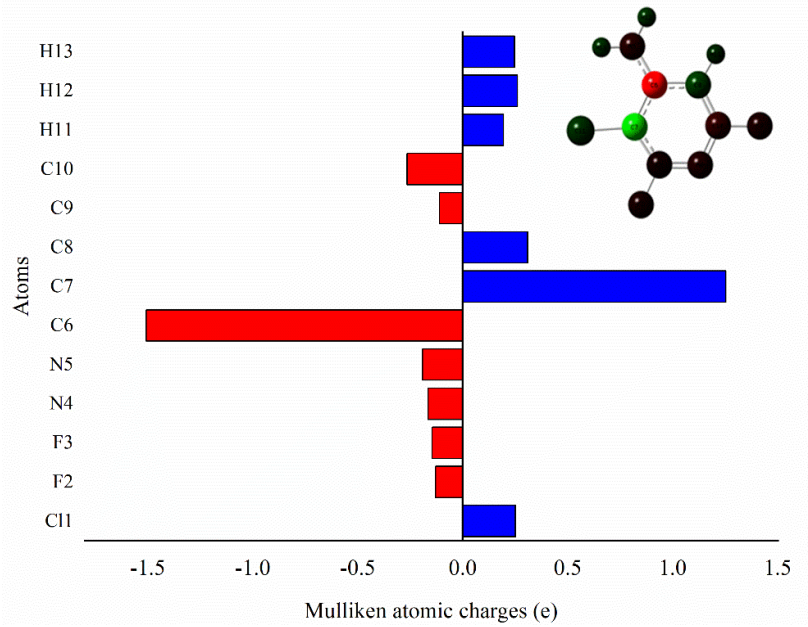

Figure 10. Mulliken charge distribution of 3C26D4A

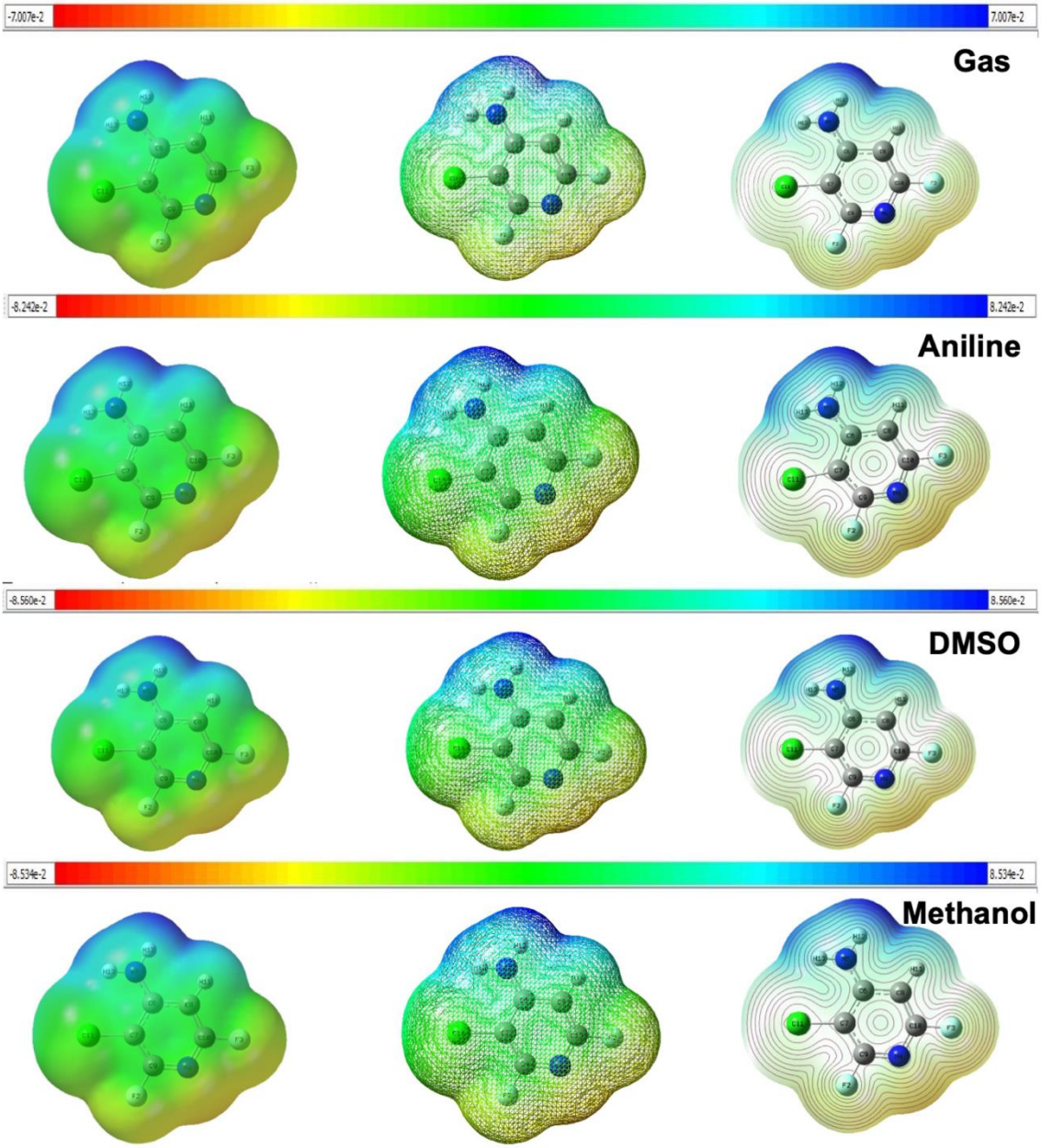
-7.007e-2
7.007e-2
Gas
-8.242e-2
8.242e-2
Aniline
-8.560e-2
8.560e-2
DMSO
-8.534e-2
8.534e-2
Methanol

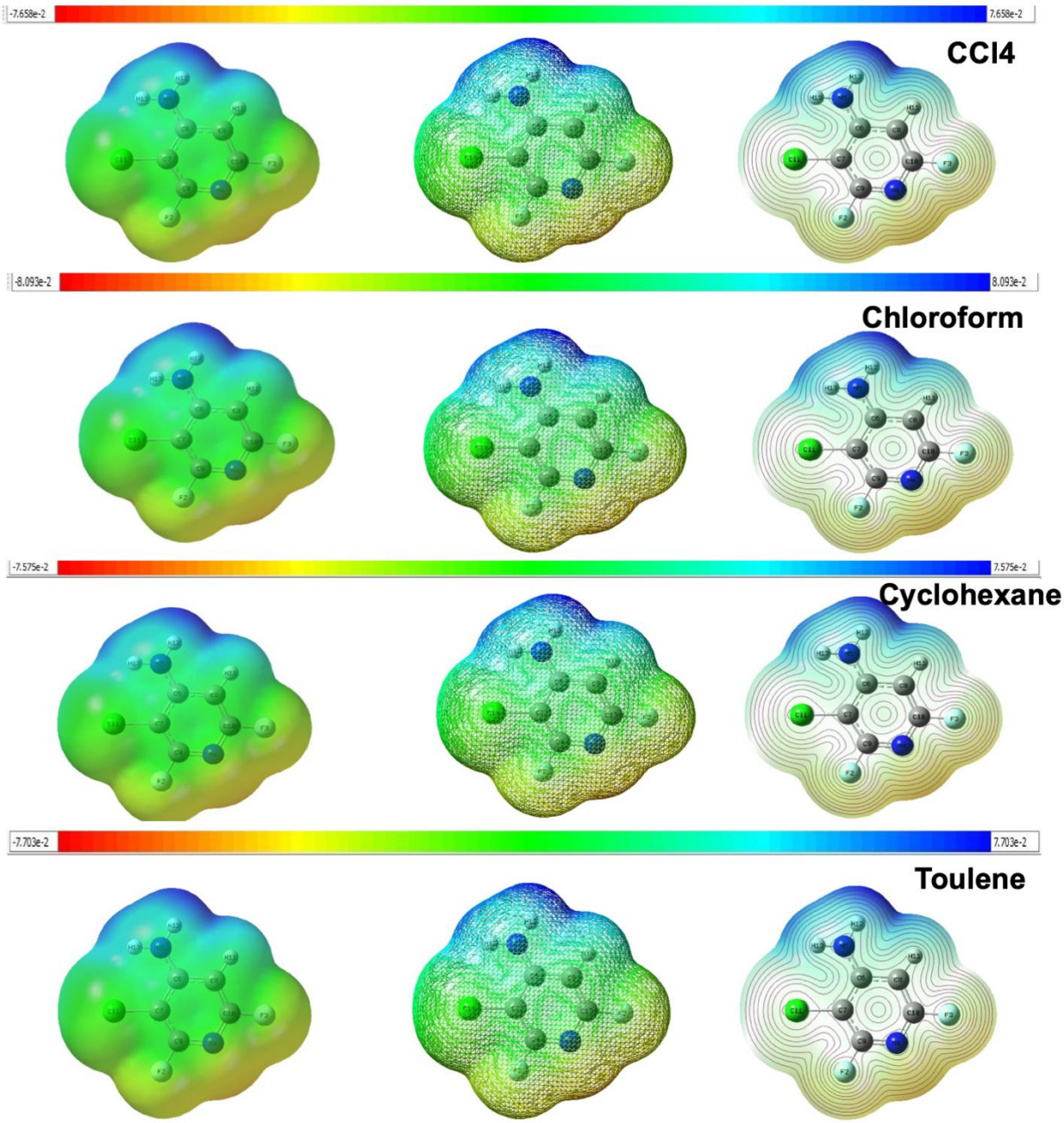

Figure 11. Total density and contour map with electrostatic potential surfaces of 3C26D4A in polar and nonpolar solvent

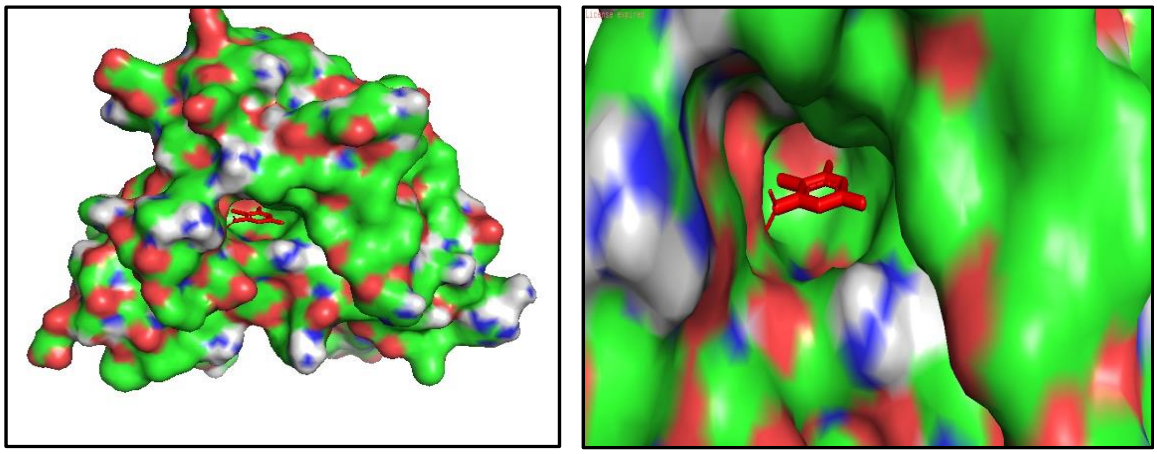

Figure 12. The 3D PyMOL view of 3C26D4A against 1KZN protein.

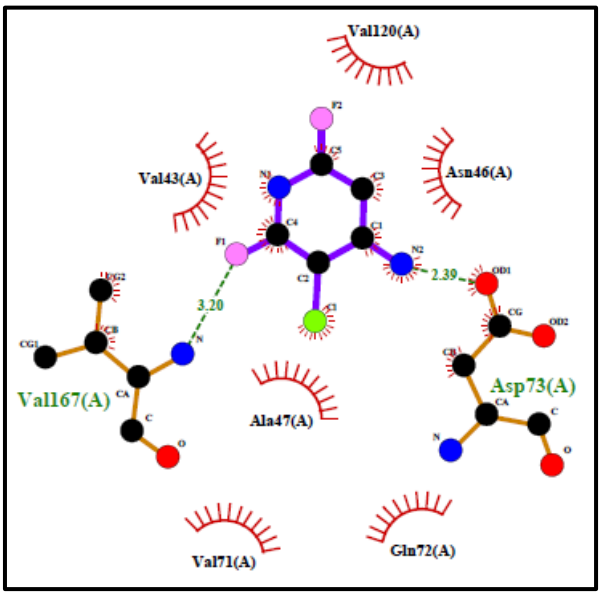

Figure 13. The 2D LigPlot+ view of 3C26D4A against 1KZN protein

Table 9. Molecular docking study of 3C26D4A against 1KZN protein

Ligand	Protein	Binding energy (kcal/mol)	No. of polar interactions	Amino acids	Bond distance (Å)	Nonpolar interaction
3C26D4A	1KZN	-4.07	2	Valine Aspartic acid	3.20 2.39	Valine 120 Asparagine 46 Valine 43 Alanine 47 Valine 171 Glutamine 72

3.8. Molecular docking

Molecular docking is a pivotal simulation technique in drug discovery, employed to anticipate and analyze how a small molecule, known as a ligand, is likely to bind and interact with a specific target macromolecule. Its fundamental objective is predicting the most favorable arrangement and conformations of the small molecule ligand within the binding site of the target macromolecule [46]. Moreover, evaluating the strength of this contact provides valuable insights into the potential efficacy and affinity of the ligand toward the target, thereby aiding in the identification and development of novel therapeutic agents. The crystal structure of macromolecule (1KZN) with specific parameters: a 2.30 Å resolution, no mutation and a single A chain comprising 205 amino acids, interacting with a complex containing single ligand clorobiocin. The molecular structure of 3C26D4A was initially drawn using GaussView 6.0, optimized without restrictions and converted to PDB format. The interaction between protein and ligand was presented in Table 9, encompassing detailed binding energy polar and nonpolar bondings. The 2D and 3D interactions were visually represented in Figures 12 and 13.

From the results, 3C26D4A creates two hydrogen bonding (polar interactions) involving amino acids valine 167 and aspartic acid 73 with a bond distance of 3.20 and 2.39 Å to the electronegative atoms fluorine and amino group, respectively. Similarly, the hydrophobic interactions (nonpolar interactions) have been made with the amino acids valine 120, 43 and 171, asparagine 46, alanine 47 and glutamine 72. These findings indicate that 3C26D4A possesses promising anti-DNA gyrase activity, a type two topoisomerase. This research may contribute to future theoretical and experimental studies involving fluorinated compounds.

4. Conclusion

Quantum chemical computational methods were employed to explore the structural, spectroscopic and electronic properties of 3C26D4A for the first time. From the investigations, the bond length of Cl_1-C_7 is increased, attributed to an electronegative group in the adjacent positions.The asymmetric stretching modes of

the amino group occur at 3573 and 3460 cm^{-1}, exhibiting a PED value of 100%. The chemical shift of carbon atoms linked to heteroatoms has increased resonance due to the deshielding effects of electronegative atoms. The simulated energy gaps were between 5.9476-5.96556 eV for polar solvents and 5.7426-6.00066 eV for nonpolar solvents. The compound is responsible for the surrounding environment's polarity by the substantial impact of solvent polarity. Furthermore, NBO analysis confirmed that the most significant stabilization of interaction energy arises from electron donation occurring from electronegative atom N_5 to the anti-bonding Carbons six and seven characterized by the LP(1)→π* transition, yielding a stabilization energy of 46.61 kJ/mol. The Mulliken population analysis revealed that the proximity of the amino group (NH_2) affects the charge distribution of the carbon atom (C6), confirmed with MESP analysis. Molecular docking unveiled interactions between ligands and macromolecules via polar bonds involving the amino group and fluorine atom of 3C26D4A with amino and carboxylic groups of the amino acids with a binding energy of -4.07 kcal/mol. These findings underscore the compound's role as a potent anti-DNA gyrase activity, emphasizing its robust antimicrobial activity.

References

[1] S.R. Alizadeh, M.A. Ebrahimzadeh, Antiviral Activities of Pyridine Fused and Pyridine Containing Heterocycles, a Review (from 2000 to 2020). Mini Reviews in Medicinal Chemistry, 21 (2021) 2584-2611. http://dx.doi.org/10.2174/1389557521666210126143558

[2] E. Vessally, A. Hosseinian, L. Edjlali, A. Bekhradnia, M.D. Esrafili, New Page to Access Pyridine Derivatives: Synthesis from: N -Propargylamines. RSC Advances, 6 (2016) 71662-71675. https://doi.org/10.1039/C6RA08720E

[3] G. Mohammad Abu-Taweel, M.M. Ibrahim, S. Khan, H.M. Al-Saidi, M. Alshamrani, F.A. Alhumaydhi, S.S. Alharthi, Medicinal importance and chemosensing applications of pyridine derivatives: a review. Critical Reviews in Analytical Chemistry, (2022) 1-18. https://doi.org/10.1080/10408347.2022.2089839.

[4] S.M. Gomha, Z.A. Muhammad, M.R. Abdel-aziz, H.M. Abdel-aziz, H.M. Gaber, M.M. Elaasser, One-pot synthesis of new thiadiazolyl-pyridines as anticancer and anti-oxidant agents. Journal of Heterocyclic Chemistry, 55 (2018) 530-536. https://doi.org/10.1002/jhet.3088

[5] T. Li, J. Zhang, J. Pan, Z. Wu, D. Hu, B. Song, Design, synthesis, and antiviral activities of 1, 5-benzothiazepine derivatives containing pyridine moiety. European journal of medicinal chemistry, 125 (2017) 657-662. https://doi.org/10.1016/j.ejmech.2016.09.069.

[6] Y. Hu, J. Zhang, C. Yu, Q. Li, F. Dong, G. Wang, Z. Guo, Synthesis, characterization, and anti-oxidant properties of novel inulin derivatives with amino-pyridine group. International journal of biological macromolecules, 70 (2014) 44-49. https://doi.org/10.1016/j.ijbiomac.2014.06.024

[7] M. Taha, N.H. Ismail, S. Imran, H. Rashwan, W. Jamil, S. Ali, S.M. Kashif, F. Rahim, U. Salar, K.M. Khan, Synthesis of 6-chloro-2-Aryl-1H-imidazo [4, 5-b] pyridine derivatives: anti-diabetic, anti-oxidant, β-glucuronidase inhibiton and their molecular docking studies. Bioorganic chemistry, 65 (2016) 48-56. https://doi.org/10.1016/j.bioorg.2016.01.007

[8] K.H. Alharbi, A review on organic colorimetric and fluorescent chemosensors for the detection of Zn (II) ions. Critical Reviews in Analytical Chemistry, 53 (2023) 1472-1488. https://doi.org/10.1080/10408347.2022.2033611

[9] D. Mohanasundaram, R. Bhaskar, M. Sankarganesh, K. Nehru, G.G.V. Kumar, J. Rajesh, A simple pyridine based fluorescent chemosensor for selective detection of copper ion. Spectrochimica Acta Part A: Molecular and Biomolecular Spectroscopy, 265 (2022) 120395. https://doi.org/10.1016/j.saa.2021.120395

[10] V. Mukherjee, K. Singh, N.P. Singh, R.A. Yadav, FTIR and Raman spectra and SQM force field calculation for vibrational analysis of 2, 3, 4-and 2, 3, 6-tri-fluoro-anilines. Spectrochimica Acta Part A: Molecular and Biomolecular Spectroscopy, 73 (2009) 44-53. https://doi.org/10.1016/j.saa.2009.01.024

[11] G.S. Kurkcuoglu, I. Kavlak, T. Arslan, C. Ogretir, Theoretical studies on the molecular structure and vibrational spectra of some dimethyl substituted pyridine derivatives. Journal of molecular modeling, 15 (2009) 79-90. https://doi.org/10.1007/s00894-008-0368-y

[12] D. Gandolfo, J. Zarembowitch, Apport de la coordination des hétérocycles a la connaissance de leurs spectres infrarouge et Raman. III—spectres de la méthyl-3 pyridine. Spectrochimica Acta Part A: Molecular Spectroscopy, 33 (1997) 615-623. https://doi.org/10.1016/0584-8539(77)80136-0

[13] J.F. Arenas, I.L. Tocon, J.C. Otero, J.I. Marcos, Vibrational spectra of methylpyridines. Journal of molecular structure, 476 (1999) 139-150.

https://doi.org/10.1016/S0022-2860(98)00541-9

[14] M. Salman, P. Sharma, M. Kumar, A.S. Ethayathulla, P. Kaur, Targeting novel sites in DNA gyrase for development of anti-microbials, Briefing Functional Genomics. 22 (2023) 180-194. https://doi.org/10.1093/bfgp/elac029

[15] A.C. Spencer, S.S. Panda, DNA Gyrase as a Target for Quinolones. Biomedicines, 11 (2023) 371. https://doi.org/10.3390/biomedicines11020371

[16] M.T. Muhammed, E. Aki-Yalcin, Computational insight into the mechanism of action of DNA gyrase inhibitors; revealing a new mechanism. Current Computer-Aided Drug Design, 20 (2024) 224-235. http://dx.doi.org/10.2174/1573409919666230419094700

[17] M.J. Frisch, G.W. Trucks, H.B. Schlegel, G.E. Scuseria, M.A. Robb, J.R. Cheeseman, G. Scalmani, V. Barone, B. Mennucci, G.A. Petersson, H. Nakatsuji, M. Caricato, X. Li, H. P. Hratchian, A. F. Izmaylov, J. Bloino, G. Zheng, J. L. Sonnenberg, M. Hada, M. Ehara, K. Toyota, R. Fukuda, J. Hasegawa, M. Ishida, T. Nakajima, Y. Honda, O. Kitao, H. Nakai, T. Vreven, J. A. Montgomery, Jr., J. E. Peralta, F. Ogliaro, M. Bearpark, J. J. Heyd, E. Brothers, K.N. Kudin, V. N. Staroverov, R. Kobayashi, J. Normand, K. Raghavachari, A. Rendell, J.C. Burant, S.S. Iyengar, J. Tomasi, M. Cossi, N. Rega, J. M. Millam, M. Klene, J. E. Knox, J. B. Cross, V. Bakken, C. Adamo, J. Jaramillo, R. Gomperts, R. E. Stratmann, O. Yazyev, A. J. Austin, R. Cammi, C. Pomelli, J. W. Ochterski, R.L. Martin, K. Morokuma, V.G. Zakrzewski, G. A. Voth, P. Salvador, J.J. Dannenberg, S. Dapprich, A. D. Daniels, Ö. Farkas, J.B. Foresman, J.V. Ortiz, J. Cioslowski, D.J. Fox (2009). GAUSSIAN09. Gaussian Inc. Wallingford, CT, USA.

[18] W. Kohn, L.J. Sham, Self-consistent equations including exchange and correlation effects. Physical Review, 140 (1965) A1133-A1138. https://doi.org/10.1103/PhysRev.140.A1133

[19] A.D. Becke, Density functional thermo chemistry – III: The role of exact exchange. The Journal of Chemical Physics, 98 (1993) 5648-5652. https://doi.org/10.1063/1.464913

[20] C. Lee, W. Yang, R.G. Parr, Development of the Colle-Salvetti correlation-energy formula into a functional of the electron density. Physical Review B, 37, (1988) 785-789. https://doi.org/10.1103/PhysRevB.37.785

[21] G.A Zhurko, & D.A. Zhurko, (2009) ChemCraft Program version 1.6 build 315.

[22] W.J. Hehre, R. Ditchfield, J.A. Pople, Self-Consistent Molecular Orbital Meth- ods. XII. Further Extensions of Gaussian-Type Basis Sets for Use in Molecular Orbital Studies of Organic Molecules. The Journal of Chemical Physics, 56 (1972) 2257–2261. https://doi.org/10.1063/1.1677527

[23] J.R. Cheeseman, G.W. Trucks, T.A. Keith, M.J. Frisch, A comparison of models for calculating nuclear magnetic resonance shielding tensors. The Journal of Chemical Physics, 104 (1996) 5497–5509. https://doi.org/10.1063/1.471789

[24] M. Petersilka, U.J. Gossman, E.K.U. Gross, Excitation energies from timedependent density-functional theory. Physical Review Letters, 76 (1966) 1212-1215. https://doi.org/10.1103/PhysRevLett.76.1212

[25] E. Runge, E.K.U. Gross, Density functional theory for time-dependent systems. Physical Review Letters, 52 (1984) 997. https://doi.org/10.1103/PhysRevLett.52.997

[26] W.L. DeLano, Pymol: An open-source molecular graphics tool. CCP4 Newsletter on protein Crystallography, 40 (2002) 82-92.

[27] R. Dennington, T. Keith, J. Millam, (2009) Gauss View, Version 5. Semichem Inc, Shawnee Mission.

[28] G.M. Morris, R. Huey, W. Lindstrom, M.F. Sanner, R.K. Belew, D.S. Goodsell, A.J. Olson, AutoDock4 and AutoDockTools4: Automated docking with selective receptor flexibility. Journal of Computational Chemistry, 30 (2009) 2785-2791. https://doi.org/10.1002/jcc.21256

[29] A.C. Wallace, R.A. Laskowski, J.M. Thornton, LIGPLOT: a program to generate schematic diagrams of protein–ligand interactions. Protein Engineering design, and selection, 8 (1995)127-134. https://doi.org/10.1093/protein/8.2.127

[30] Tamara A. Vaganova, Yurij V. Gatilov, Enrico Benassi, Igor P. Chuikov, Denis P. Pishchur, Evgenij V. Malykhin CCDC 1911495: Experimental Crystal Structure Determination. 2019, 10.5517/ccdc.csd.cc22524h

[31] G. Serdaroglu, N. Uludag, N. Colak, P. Rajkumar, Nitrobenzamido substitution on thiophene-3-carboxylate: Electrochemical investigation, antioxidant activity, molecular docking, DFT calculations. Journal of Molecular Structure, 1271 (2023) 134030. https://doi.org/10.1016/j.molstruc.2022.134030

[32] S. Selvaraj, A. Ram Kumar, T. Ahilan, M. Kesavan, G. Serdaroglu, P. Rajkumar, M. Mani, S. Gunasekaran, S. Kumaresan, Experimental and Theoretical Spectroscopic Studies of the Electronic Structure of 2-Ethyl-2-phenylmalonamide. Physical Chemistry Research, 10 (2022) 333-344.

[33] P. Wojciechowski, K. Helios, D. Michalska, Theoretical anharmonic Raman and infrared spectra with vibrational assignments for monofluoroaniline isomers. Vibrational Spectroscopy, 57 (2011) 126-134. https://doi.org/10.1016/j.vibspec.2011.06.001

[34] P. Rajkumar, S. Selvaraj, R. Suganya, M. Kesavan, G. Serdaroglu, S. Gunasekaran, S.Kumaresan, Experimental and theoretical investigations on electronic structure of 5-(hydroxymethyl)-2-furaldehyde: An antisickling agent identified from Terminalia bellirica. Chemical Data Collections, 29, (2020) 100498. https://doi.org/10.1016/j.cdc.2020.100498

[35] A. Ram Kumar, S. Selvaraj, G.S. Mol, M. Selvaraj, L. Ilavarasan, S.K. Pandey, P. Jayaprakash, S. Awasthi, O. Albormani, A. Ravi, Synthesis, solvent-solute interactions (polar and nonpolar), spectroscopic insights, topological aspects, Fukui functions, molecular docking, ADME, and donor-acceptor investigations of 2-(trifluoromethyl) benzimidazole: A promising candidate for antitumor pharmacotherapy. Journal of Molecular Liquids, 393, (2024) 123661. https://doi.org/10.1016/j.molliq.2023.123661

[36] S. Seshadri, S. Gunasekaran, S. Muthu, S. Kumaresan, R. Arun Balaji, Vibrational spectroscopy investigation using ab initio and density functional theory on flucytosine. Journal Raman Spectroscopy, 38(11), (2007) 1523-1531. https://doi.org/10.1002/jrs.1808

[37] S. Gunasekaran, K. Rajalakshmi, S. Kumaresan, Vibrational analysis, electronic structure and nonlinear optical properties of Levofloxacin by density functional theory. Spectrochimica Acta Part A: Molecular and Biomolecular Spectroscopy, 112, (2013) 351-363. https://doi.org/10.1016/j.saa.2013.04.074

[38] A. Ram Kumar, S. Selvaraj, P. Anthoniammal, R.J. Ramalingam, B. Ranjith, P. Jayaprakash, G.P. Sheeja Mol, Comparison of spectroscopic, structural, and molecular docking studies of 5-nitro-2-fluoroaniline and 2-nitro-5-fluoroaniline: An attempt on fluoroaniline isomers. Journal of Fluorine Chemistry, 270, (2023) 110167. https://doi.org/10.1016/j.jfluchem.2023.110167

[39] M. Karabacak, E. Kose, E.B. Sas, M. Kurt, A.M. Asiri, A. Atac, DFT calcula- tions and experimental FT-IR, FT-Raman, NMR, UV–Vis spectral studies of 3- fluorophenylboronic acid. Spectrochimica Acta Part A: Molecular and Biomolecular Spectroscopy, 136 (2015) 306-320. https://doi.org/10.1016/j.saa.2014.08.141

[40] R.V. Kabilan, C. Arunagiri, G.R. Ramkumaar, K. Sathyamoorthy, C. Karnan, Combined experimental and theoretical investigations on 9-[3, 4-dihydroxy-5-(hydroxymethyl) oxolan-2-yl]-1, 9-dihydro-6H-purin-6-one 4-nitrophenol (IPNP) molecule. Journal of Molecular Structure, 1263, (2022) 133020. https://doi.org/10.1016/j.molstruc.2022.133020

[41] A. Gokila, Comprehensive understanding of Methyl 2-Naphthyl Ether Molecule by Ab Initio Calculation method. International Research Journal of Multidisciplinary Technovation, 5(1), (2023) 19-33. https://doi.org/10.54392/irjmt2323

[42] A. Mohamed Ibrahim, S. Arunachalam, J. Suryakanth, M. Velayutham Pillai, A Quantum Chemical and Nonlinear Optical Investigation on L-Tryptophan Hydrochloride Single Crystals for Optoelectronic Device Applications. International Research Journal of Multidisciplinary Technovation, 5(4), (2023) 20-26, https://doi.org/10.54392/irjmt2343

[43] M. Prabhaharan, A.R. Prabakaran, S. Gunasekaran, S. Srinivasan, Molecular structure and vibrational spectroscopic investigation of melamine using DFT theory calculations. Spectrochimica Acta Part A: Molecular and Biomolecular Spectroscopy, 123, (2014) 392-401. https://doi.org/10.1016/j.saa.2013.12.056

[44] S. Selvaraj, Computational study on the structural features, vibrational aspects, chemical shifts, and electronic properties of 1,4-Dinitrosopiperazine-2-carboxylic acid: Insights into donor-acceptor interactions and thermodynamic properties. International Research Journal of Multidisciplinary Technovation, 6(1), (2024) 1-16. https://doi.org/10.54392/irjmt2411

[45] C. Karnan, K.S. Nagaraja, S. Manivannan, A. Manikandan, V. Ragavendran, Crystal structure, spectral investigations, DFT and antimicrobial activity of brucinium benzilate (BBA). Journal of Molecular Modeling, 27, (2021) 1-11. https://doi.org/10.1007/s00894-021-04842-w

[46] E. Dhanalakshmi, P. Rajesh, S. Suresh, M. Priyadharshini, M. Prabhaharan, Green synthesis, spectroscopic investigation, quantum chemical and molecular docking studies of 3-

methylisoxazolo [4,5-b] pyridine. Journal of Molecular Structure, 1298, (2024) 136964. https://doi.org/10.1016/j.molstruc.2023.136964

Authors Contribution Statement

S. Kavi Karunya: Methodology, Writing – Review & Editing, Investigation, Supervision: **K. Jagathy**: Conceptualization, Formal analysis, Writing Original Draft; **K. Anandaraj**: Methodology, Data curation, Investigation; **C. Pavithra**: Formal Analysis, Visualization, Validation; **R. Manjula**: Data Curation, Visualization. All the authors read and approved the final version of the manuscript.

Availability of data:

Data will be made available on request.

Conflict of Interest:

The authors report there are no competing interests to declare.

Has this article screened for similarity?

Yes

About the License